JOURNAL OF SOLID STATE CHEMISTRY 27, 115–122 (1979)

Fluorite-Related Phases Ln_3MO_7, Ln = Rare Earth, Y or Sc, M = Nb, Sb, or Ta

II. Structure Determination

H. J. ROSSELL

CSIRO, Division of Materials Science, Engineering Ceramics and Refractories Laboratory, P.O. Box 4331, GPO, Melbourne 3001, Victoria, Australia

Received March 11, 1978

The crystal structures of the orthorhombic fluorite-related compounds La_3NbO_7 (*Cmcm*), Y_3TaO_7, and Y_2GdSbO_7, ($C222_1$) have been determined from X-ray powder diffraction intensities and single-crystal electron diffraction data. The structures are basically similar. One third of the *Ln* cations are 8-coordinated, and lie in [001] rows which alternate with parallel rows of corner-linked MO_6 coordination octahedra within slabs parallel to (100). The remaining *Ln* cations lie in between these slabs in seven-fold coordination. This interslab cation arrangement distinguishes the structure from the closely related pyrochlore ($A_2B_2O_7$) and weberite (Na_2MgAlF_7) structures. The compounds $YGdScSbO_7$ and Nd_2ScNbO_7, also examined, have the pyrochlore structure, with Sc and Sb, or Sc and Nb distributed on the octahedral *B* sites.

Introduction

The crystal chemistry of some fluorite-related compounds Ln_3MO_7, with Ln = rare earth, Y, or Sc, and M = Nb, Sb or Ta, has been described in Part I (*1*). The present paper describes the determination of the crystal structures of four compounds representative of the orthorhombic Ln_3MO_7 phase, and a confirmatory determination of two Ln_2ScMO_7 pyrochlores.

Experimental

The preparation of the Ln_3MO_7 compounds has been described in Part I. The particular specimens examined here were as follows:

La_3NbO_7: sintered from the component oxides at 1400°C for 7 days.

Nd_3NbO_7: (a) arc-melted and annealed at 1400°C for 40 h; (b) coprecipitated and fired at 1400°C for 14 days; (c) component oxides sintered at 1400°C for 14 days; (d) component oxides sintered at 1350°C for 1 day, then 1260°C for 7 days.

Y_2GdSbO_7 and $YGdScSbO_7$: component oxides reacted at 960°C for 16 hr then heated at 1200°C for 24 hr, and 1350°C for 72 hr.

Nd_2ScNbO_7: component oxides sintered at 1400°C for 14 days.

Y_3TaO_7: component oxides sintered at 1400°C for 40 days.

Single-crystal electron diffraction patterns were used to indicate the symmetry of the orthorhombic phases; these patterns have been discussed in Part I.

Powder X-ray diffraction intensities (Ni-

0022-4596/79/0271/0115/08/$02.00/0

filtered Cu$K\alpha$ radiation) were recorded on chart using a counter diffractometer which was operated in continuous scan mode. Areas of peaks were measured with a planimeter. All reflections up to $2\theta = 90°$ (orthorhombic phase) or $2\theta = 160°$ (pyrochlores) were included in the data. Unresolved groups of reflections were generally treated as single observations. However, some such groups of peaks were resolved clearly on Guinier photographs, in which case the observed intensity was distributed among the relevant reflections in proportion to the peak heights on a microdensitometer trace of the photograph. No extra corrections for differing *Lp* factors were considered necessary.

The data from the various specimens of Nd_3NbO_7 differed only in insignificant details, and so they were averaged into one set.

Structure refinement was carried out using a least-squares computer program based on ORFLS (*2*), which is appropriate for the treatment of powder data. The quantity minimized is $\sum w(I_o - I_c)^2$, where $w = k/(I_o + I_{min})$, I_{min} is about equal to the smallest observable intensity, and k is a multiplier, usually unity, which may reflect reduced confidence in any particular observation. The residual R used here is $\frac{1}{2}[\sum w(I_o - I_c)^2/\sum wI_o^2]^{1/2}$; it is numerically comparable to the weighted residual commonly quoted for structure refinements based on F.

Scattering factors for neutral atoms were used (*3*), with corrections for anomalous dispersion (*4*). Where more than one atom type occupied a given set of equivalent positions, appropriately weighted means of scattering factors and anomalous dispersion corrections were taken.

An overall isotropic temperature factor of zero was used. If refined, the value remained close to zero and was accompanied by relatively large calculated standard deviations, and it is probable that, for the orthorhombic phases especially, it reflected the condition of the specimen surface rather than the effect of thermal motion.

Structure Determination

For Y_3TaO_7, Y_2GdSbO_7, and Nd_3NbO_7, the only condition limiting reflections in the electron diffraction patterns was $h + k = 2n$ for all *hkl*, so that the space group is one of the set *Cmmm* (No. 65, D_{2h}^{19}), *Cm2m*, or *C2mm* (settings of *Amm2*, No. 38, C_{2v}^{19}), *Cmm*2 (No. 35, C_{2v}^{11}), *C*222 (No. 21, D_2^6), or, since double diffraction can obscure the condition *l* even for 00*l*, $C222_1$ (No. 20, D_2^5). The condition on 00*l* applied, as far as could be seen, in the X-ray diffraction data. For La_3NbO_7, there was in addition to the above, the condition $l = 2n$ for *h*0*l*, making the space group one of *Cmcm* (No. 63, D_{2h}^{17}), *C*2*cm* (a setting of *Ama*2, No. 40, C_{6v}^{16}), or $Cmc2_1$ (No. 36, C_{2v}^{12}). The unit cells contain four fluorite M_4O_8 units [Part I, Eq. (1)] and thus have the contents $M_{16}O_{28}V_4$ (V = oxygen vacancy), an assignment confirmed by the agreement of calculated densities with those measured by a buoyancy method (*5*).

Atoms were assumed to be initially in the ideal fluorite-derived positions within the unit cell, with all the anion sites occupied and with the cations ordered. Each space group permitted a number of different cation arrangements, and in addition, the relative position of the origin often could be chosen in several ways so as to give different sets of atomic parameters that could be varied during refinement.

Refinement of scale factor and appropriate atomic parameters was carried out for each of these models. Some initial shifts of atoms were required in order to remove degeneracy in the models before refinement would proceed, and all possible permutations of these shifts were tried.

For Y_3TaO_7 and Y_2GdSbO_7, refinement of one model in $C222_1$ converged rapidly, producing a low value for the residual and acceptably low values for the calculated standard deviations of refined parameters, whereas refinement of other models in this space group, or refinements in the more

positively indicated space groups either did not converge, or yielded residuals higher than 0.10. Moreover, the structure in $C222_1$ was reasonable from the crystal chemistry standpoint.

In the case of La_3NbO_7, only one model, in *Cmcm*, produced a satisfactory refinement result. The convergence was not as rapid, nor was the residual as small as in the two cases above, an effect perhaps attributable to the accuracy of the data. Refinement results from the other possible models were rejected either because of a high residual, or in the case of some noncentric models, because the result corresponded to essentially the same structure as that in *Cmcm*, but represented no significant improvement in the fit of observed and calculated intensities.

For Nd_3NbO_7, no model in any of the formally possible space groups gave a satisfactory result, but success was achieved using *Cmcm*, a space group from the set indicated for La_3NbO_7. Models in the other space groups of this set were tried also, with results that were similar to those obtained under the same conditions for La_3NbO_7. The reflections $h0l$ with l odd were not absent in the electron diffraction patterns from Nd_3NbO_7, but they were extremely weak (Part I, Fig. 1b). It was considered unlikely that they arose by double diffraction from the adjacent Laue zone, i.e., the next level, since this effect was not observed under similar conditions for La_3MO_7. No intensity above background was measured for these reflections in the X-ray powder data, in contrast to the cases of Y_3TaO_7 and Y_2GdSbO_7, and it was concluded that since the conditions for a *c* glide were so nearly established, the structure in *Cmcm* represented a reasonable approximation to the true one. The several independent data sets all gave essentially the same results.

The location of the vacant anion sites in Y_3TaO_7 and Y_2GdSbO_7 was straight forward: The occupancy of an oxygen atom on a fourfold site dropped to zero when oxygen occupancies were refined, while the remainder were unaffected. For La_3NbO_7 and Nd_3NbO_7, this did not occur. Instead, for a trial oxygen atom placed initially at position 8*g* in *Cmcm*, i.e., at $(x,y,\frac{1}{4})$ with $x = \frac{1}{8}$ and $y = \frac{1}{2}$, the x parameter shifted toward zero and the occupancy became halved, indicating that this atom was located at the fourfold site 4*c*, viz., $(0,y,\frac{1}{4})$ with $y \simeq \frac{1}{2}$.

Pyrochlore Phases

The pyrochlore structure, adopted typically by compounds $A_2B_2O_7$, has been well documented (*6*, *7*). The unit cell, space group $Fd3m$, may be regarded as consisting of eight fluorite subcells in a 2 × 2 × 2 array: The cations are ordered, and there is one formal anion vacancy per subcell. There are 16 *A* cations at equipoints (*d*) $(\frac{1}{2},\frac{1}{2},\frac{1}{2})$, 16 *B* cations at (*c*) (0,0,0), 8 anions at (*b*) $(\frac{3}{8},\frac{3}{8},\frac{3}{8})$, 48 anions at (*f*) $(x,\frac{1}{8},\frac{1}{8})$ and 8 formal anion vacancies at (*a*) $(\frac{1}{8},\frac{1}{8},\frac{1}{8})$. The single variable positional parameter usually lies in the range $0.305 \leqslant x \leqslant 0.338$; the values $x = 0.3125$ or $x = 0.375$ result in structures with regular octahedra of O around *B* or regular cubes of O around *A*, respectively.

In the present cases, there was an additional variable parameter to account for the distribution of cations on the sites *A* and *B*. Initially, all the cations were assumed to be distributed randomly on both sites, and the positional parameter was chosen to give a regular octahedron of O about the *B* site. During refinement, changes in *B* site occupancy were assessed in terms of actual atoms on *A* and *B* sites, and suitable adjustments made to the composite scattering factors and dispersion corrections.

Results and Discussion

The results from the structure refinements of the orthorhombic phases are given in Table I, and some derived data in Table II, while Figs. 1 and 2 show perspective views of the two structure types exemplified by La_3NbO_7 and Y_3TaO_7.

TABLE I

ATOMIC COORDINATES FOR THE ORTHORHOMBIC STRUCTURES[a,b]

Nd_3NbO_7

$a = 10.905(2)$; $b = 7.517(2)$; $c = 7.624(1)$ Å
Space group $Cmcm$, 92 observations, $R = 0.0546$

Atom	Point set	x	y	z
Nb	4*b*	0	½	0
Nd	4*a*	0	0	0
Nd II	8*g*	0.2267(6)	0.2969(7)	¼
O I	16*h*	0.125(4)	0.321(6)	−0.036(5)
O II	8*g*	0.161(6)	0.013(8)	¼
O III	4*c*	0	0.450(11)	¼

La_3NbO_7

$a = 11.167(1)$; $b = 7.629(1)$; $c = 7.753(1)$ Å
Space group $Cmcm$, 89 observations, $R = 0.0602$

Atom	Point set	x	y	z
Nb	4*b*	0	½	0
La I	4*a*	0	0	0
La II	8*g*	0.2253(6)	0.3025(8)	¼
O I	16*h*	0.129(5)	0.320(6)	−0.036(5)
O II	8*g*	0.139(6)	0.028(8)	¼
O III	4*c*	0	0.449(11)	¼

Y_3TaO_7

$a = 10.4762(7)$; $b = 7.4237(7)$; $c = 7.4522(5)$ Å
Space group $C222_1$, 71 observations, $R = 0.0362$

Atom	Point set	x	y	z
Ta	4*b*	0	0	¼
Y I	4*b*	0	0.494(3)	¼
Y II	8*c*	0.2360(6)	0.2379(9)	0.000(1)
O Ia	8*c*	0.143(9)	0.185(9)	0.278(13)
O Ib	8*c*	0.108(8)	0.773(11)	0.292(14)
O IIa	4*a*	0.130(10)	½	0
O IIb	4*a*	0.149(10)	½	½
O III	4*a*	0.077(8)	0	0
(Vacancy)	4*a*	−⅛	0	0

Y_2GdSbO_7

$a = 10.5172(6)$; $b = 7.4527(5)$; $c = 7.4806(4)$ Å
Space group $C222_1$, 70 observations, $R = 0.0404$

Atom	Point set	x	y	z
Sb	4*b*	0	0	¼
0.374Y + 0.626Gd (*Ln* I)	4*b*	0	0.487(2)	¼
0.813Y + 0.187Gd (*Ln* II)	8*c*	0.2331(6)	0.2343(10)	0.009(1)
O Ia	8*c*	0.129(9)	0.205(9)	0.285(9)
O Ib	8*c*	0.132(8)	0.800(9)	0.299(10)
O IIa	4*a*	0.137(10)	½	0
O IIb	4*a*	0.141(10)	½	½
O III	4*a*	0.062(9)	0	0
(Vacancy)	4*a*	−⅛	0	0

[a] Numbers in parentheses are estimated standard deviations, which apply to the last quoted places.
[b] Supercell axes in terms of fluorite subcell axes: 200/011/0$\bar{1}$1.

The orthorhombic structures have features in common. Thus slabs may be recognised, parallel to (100), in which rows of *M* cations in octahedral coordination by O, lie in the direction [001] alternating with parallel rows of *Ln* I cations in eight-fold coordination. Slabs are stacked with all rows parallel, and between the slabs are *Ln* II cations in seven-fold coordination. It is emphasized that the slabs are descriptive only, and no difference in *Ln* II–O bonding is implied.

The possibility that the *Ln* I and *Ln* II cations may be of different type, the 7-coordinated *Ln* II being the smaller, is realized in Y_2GdSbO_7. The cation ordering in this specimen was not complete, and it is possible that longer annealing times with protection against Sb_2O_3 losses would allow complete ordering to occur.

The shapes of the coordination polyhedra about the cations may be assessed from Table II and Figs. 1 and 2. In particular, it may be noticed that in La_3NbO_7 and Nd_3NbO_7, the MO_6 octahedra and LnO_8 cubes are more nearly regular than in the other two structures, and that the polyhedron about the *Ln* II cation can be represented by seven of the eight vertices of a distorted cube in Y_3TaO_7 and Y_2GdSbO_7 and by a pentagonal bipyramid in La_3NbO_7 and Nd_3NbO_7.

The two orthorhombic structures have other differences in oxygen substructure, most notably in the position of O III, which causes the difference in the way the MO_6 octahedra are tilted with respect to the cell axes. In Y_3TaO_7 and Y_2GdSbO_7, O III lies reasonably close to the ideal fluorite position $(\frac{1}{8}, 0, 0)$, and it is associated with an anion site at $(-\frac{1}{8}, 0, 0)$ that

TABLE II

SOME INTERATOMIC DISTANCES AND ANGLES[a]

	$C222_1$			*Cmcm*	
	Y_3TaO_7	Y_2GdSbO_7		Nd_3NbO_7	La_3NbO_7
Polyhedron about M:					
M–O Ia	2 of 2.05	2.06	M–O I	4 of 1.93	2.01
–O Ib	2 of 2.05	2.08			
–O III	2 of 2.03	1.98	–O III	2 of 1.96	1.98
O III–M–O Ia	79	84	O III–M–O I	88	90
O III–O Ia	2.58	2.71	O III–O I	2.71	2.82
O III–M–O Ib	85	87			
O III–O Ib	2.77	2.79			
O Ia–M–O Ib	98	94	O I–M–O I′	91	89
O Ia–O Ib	3.08	3.02	O I–O I′	2.77	2.81
Polyhedron about *Ln* I:					
Ln I–O Ia	2 of 2.43	2.52	*Ln* I–O I	4 of 2.80	2.84
–O Ib	2 of 2.75	2.74			
–O IIa	2 of 2.31	2.37	–O II	4 of 2.60	2.49
–O IIb	2 of 2.38	2.39			
O Ia–*Ln* I–O Ia′	67	66	O I–*Ln* I–O I′	58	61
O Ib–*Ln* I–O Ib′	59	64			
O Ia–*Ln* I–O IIa	76	77	O I–*Ln* I–O II	72	72
O Ia–*Ln* I–O IIb	67	68	O I–*Ln* I–O II′	70	72
O IIa–*Ln* I–O IIb	76	76	O II–*Ln* I–O II′	84	77
Mean edge O–O	2.90	2.88	Mean edge O–O	3.13	3.09
Polyhedron about *Ln* II:[b]					
Ln II–O Ia	2.16	2.27	*Ln* II–O I	2 of 2.40	2.47
–O Ia′	2.32	2.35			
–O Ib	2.27	2.08	–O I′	2 of 2.51	2.51
–O Ib′	2.56	2.54			
–O IIa	2.24	2.22	–O II	2.05	2.30
–O IIb	2.14	2.20	–O II′	2.27	2.31
–O III	2.43	2.50	–O III	2.72	2.75
O Ia–*Ln* II–O Ib	73	74	O III–*Ln* II–O I	2 of 64	65
O Ia–*Ln* II–O Ib′	70	68	O I–*Ln* II–O I′	2 of 73	73
O Ia–*Ln* II–O III	65	68	O I′–*Ln* II–O I″	86	83
O Ia–*Ln* II–O IIa	87	84	O II–*Ln* II–O I	2 of 85	81
O Ib′–*Ln* II–O IIb	72	78	O II′–*Ln* II–O I	2 of 86	86
Vacancy–M	2 of 2.78	2.48			
Vacancy–*Ln* II	2 of 2.43	2.29			
M–O (fluorite)[c]	2.274	2.283		2.342	2.376
Vacancy–O Ia	2 of 2.16	2.22			
–O Ib	2 of 2.30	2.12			
–O IIa	2.56	2.50			
–O III	2.12	1.97			
O–O (fluorite)[c]	2.625	2.636		2.704	2.743

[a] Distances are given in Angstroms, and angles in degrees. Estimated standard deviations, as fractions of the relevant values, are commonly: metal–oxygen, 1–2%, oxygen–oxygen, 2–3%, angle oxygen–metal–oxygen, 3–4%.

[b] For the structures in *Cmcm*, the mean plane through atoms *Ln* II, the four O I and O III is nearly parallel to (320), and the distances of these atoms from the plane are all less than 1.2 σ, $\sigma = 0.15$ A.

[c] Fluorite distances have been calculated for a cell one quarter of the volume of the relevant supercell.

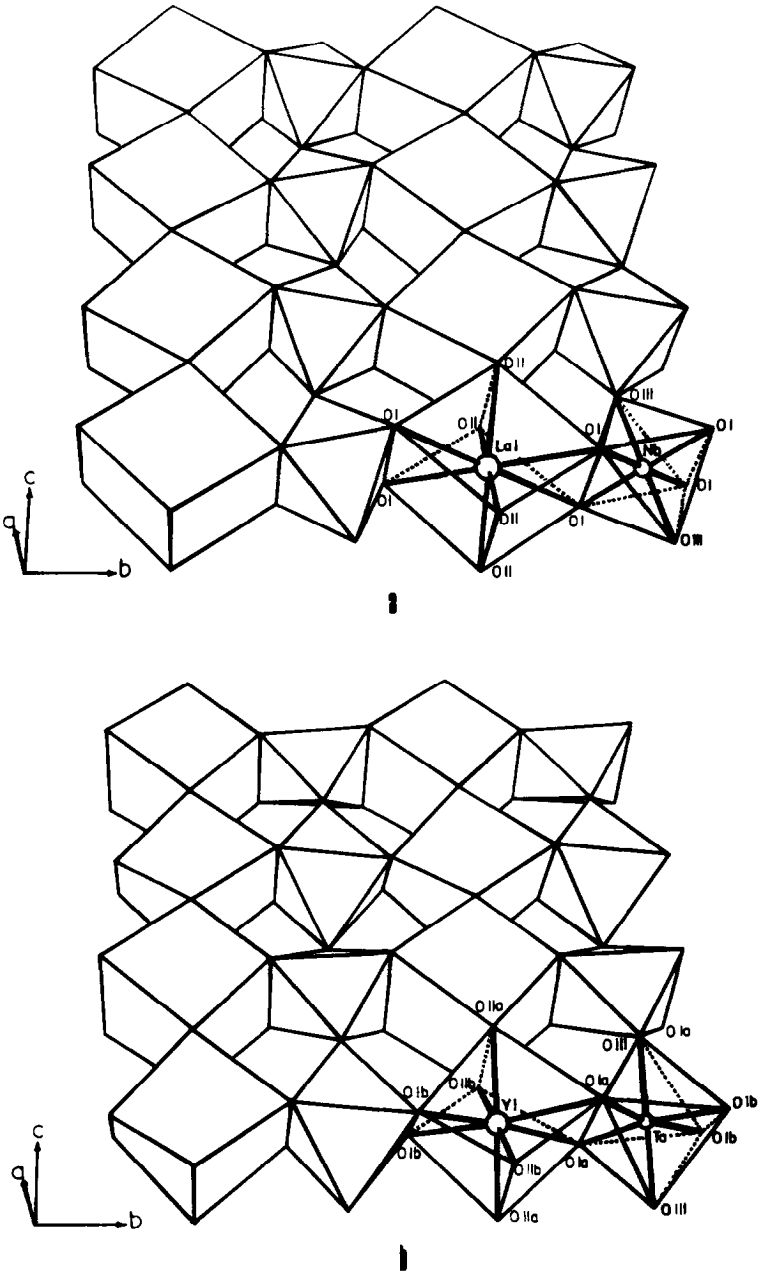

FIG. 1. Arrangement of $Ln(I)O_8$ cubes and MO_6 octahedra in (100) slabs in Ln_3MO_7 of the two structure types: (a) La_3NbO_7, (b) Y_3TaO_7.

is formally vacant, compared to the ideal fluorite subcell. (If each vacant site were occupied, the polyhedron about *M* would be a cube similar to that about *Ln* I). Anions adjacent to the vacancy have relaxed towards it by up to 0.5 Å, while the tetrahedron of cations surrounding it has dilated, compared to the ideal fluorite case. These conditions are

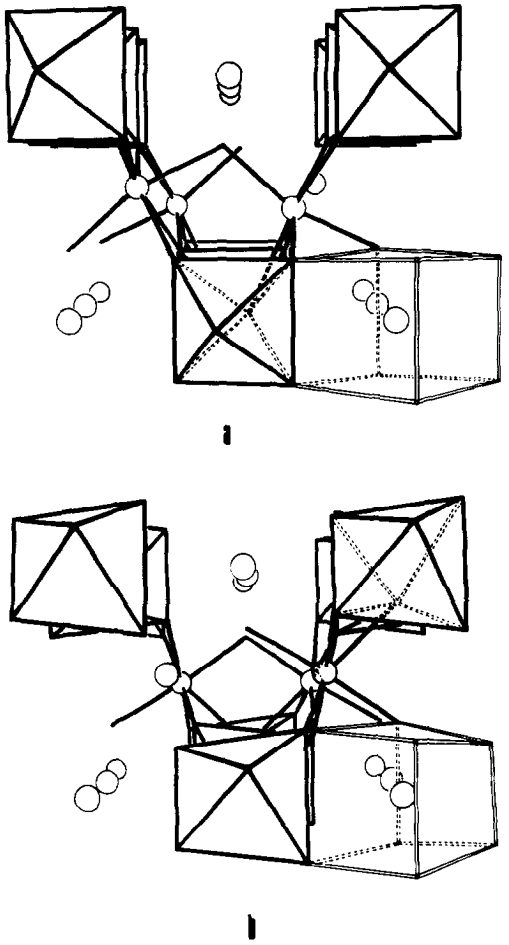

FIG. 2. La_3NbO_7 (a) and Y_3TaO_7 (b), viewed along the rows of *M* and *Ln* I cations, viz., [001] or [01$\bar{1}$] (fluorite), showing interslab *Ln* II cation coordination. The coordination of one *Ln* II cation is not drawn. The remaining circles represent the 8-coordinated *Ln* I cations.

TABLE III

ATOMIC PARAMETERS FOR THE PYROCHLORE PHASES[a]

Atom	Nd_2ScNbO_7	$YGdScSbO_7$
B at (0, 0, 0)	0.5Sc + 0.5Nb	0.5Sc + 0.5Sb
A at ($\frac{1}{2}$, $\frac{1}{2}$, $\frac{1}{2}$)	Nd	0.5Y + 0.5Gd
O I at ($\frac{3}{8}$, $\frac{3}{8}$, $\frac{3}{8}$)		
O II at (x, $\frac{1}{8}$, $\frac{1}{8}$): x	0.330(3)	0.337(2)
No. of observations	50	48
R	0.0432	0.0384

[a] Space group $Fd3m$. Origin at center.

characteristic of ordered fluorite-related superstructures (*9*, *10*) and are to be expected on electrostatic grounds.

By contrast, anion vacancies of this type do not occur in La_3NbO_7 and Nd_3NbO_7. Here, the O III anion has shifted from its ideal position by a relatively large amount, and lies

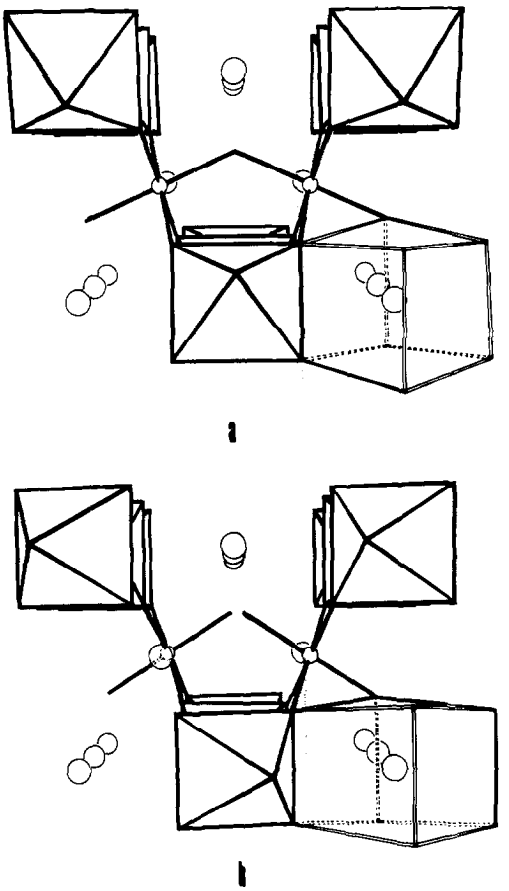

FIG. 3. (a) The pyrochlore structure, in this case, Nd_2ScNbO_7, viewed along [110], i.e., [110] (fluorite). Large circles represent the A cations (Nd) in 8-fold coordination by O, and the two small circles the 6-coordinated *B* cations (which also exist at the centres of the octahedra). The cubic symmetry of pyrochlore has been obscured in the figure: The interslab cation arrangement in fact is identical to that in the slabs, but rotated 90° about a vertical axis. (b) [100], i.e., [011] (fluorite) view of the weberite structure, drawn from the data for $Ca_2Sb_2O_7$ given by Byström (*12*). The large circles represent the 8-coordinated Ca cations. Compared to (a), the interslab cations are arranged diagonally, and interslab octahedra are linked only to those in adjacent slabs.

midway between the two fluorite positions that were associated with O III and the vacancy in the other two compounds.

In Y_3TaO_7 and Y_2GdSbO_7, therefore, a vacancy pair, separated by a $\frac{1}{2}[111]$ fluorite lattice vector and with a cation (M) in between, may be recognized. This unit also is characteristic of other fluorite-related superstructures examined so far. Each vacancy is associated with two M cations, so that infinite zigzag chains of vacancy pairs occur parallel to [001], i.e., to the $[01\bar{1}]$ fluorite subcell direction. This type of configuration occurs also in pyrochlore, but there the chains run in all the $\langle 110 \rangle$ fluorite subcell directions.

Table III contains the results of the structure refinements of the pyrochlores Nd_2ScNbO_7 and $YGdScSbO_7$. Since these determinations were only confirmatory (Part I), it may be noted merely that the value of the single variable positional parameter lies in the range 0.305 to 0.338 typical of other pyrochlores, and corresponds to an approximately regular octahedral coordination by O of the B site, which is occupied by the smaller pair of cations.

The orthorhombic Ln_3MO_7 structures are related closely to the pyrochlore and weberite (Na_2MgAlF_7) (*11*, *12*) structures, representations of which are shown in Fig. 3. By comparing Figs. 2 and 3, in which all structures are shown viewed along the same subcell direction, it can be seen that they have a similar arrangement of MO_6–LnO_8 slabs, and differ basically only in the interslab cation configuration. In Ln_3MO_7, the interslab cations are all equivalent, and are 7-coordinated, whereas in pyrochlore and weberite, there are equal numbers of two types, 6- and 8-coordinated, but in different arrangements. In view of these structural similarities, pseudobinary solid solution phases with perhaps additional ordering effects may be envisaged: Their structural investigation may be of some interest.

Thus the compounds Ln_3MO_7 exhibit many of the structural features found in other fluorite-related superstructures. The frequently observed octahedral coordination of M cations is demonstrated in the present cases, and for La_3NbO_7 and Nd_3NbO_7, a large relaxation of the oxygen substructure from the fluorite type has been necessary to achieve this.

Acknowledgment

The author wishes to acknowledge the assistance given to this work by Mr. J. G. Allpress, formerly of this Division.

References

1. J. G. Allpress and H. J. Rossell, *J. Solid State Chem.* **27**, 00 (1978).
2. W. R. Busing, K. O. Martin, and H. A. Levy, ORNL-TM-305 (1962).
3. D. T. Cromer and J. T. Waber, *Acta Crystallogr.* **18**, 104 (1965).
4. D. T. Cromer and D. Liberman, *J. Chem. Phys.* **53**, 1891 (1970).
5. W. W. Barker, *J. Appl. Crystallogr.* **5**, 433 (1972).
6. E. Aleshin and R. Roy, *J. Amer. Ceram. Soc.* **45**, 18 (1962).
7. F. Brisse and O. Knop, *Canad. J. Chem.* **46**, 859 (1968).
8. J. G. Allpress, H. J. Rossell, and H. G. Scott, *J. Solid State Chem.* **14**, 264 (1975).
9. H. J. Rossell, *J. Solid State Chem.* **19**, 103 (1976).
10. H. J. Rossell and H. G. Scott, *J. Solid State Chem.* **13**, 345 (1975).
11. A. Byström, *Ark. Kem. Min. Geol.* **18B**, No. 10 (1944).
12. A. Byström, *Ark. Kem. Min. Geol.* **18A**, No. 21 (1944).